Journal of Physics:
Conference Series

PAPER • **OPEN ACCESS**

Effect of Sawtooth Current Waveform on Plasma Dynamics in Electrothermal PPT: A Simulation Approach

To cite this article: Marwa. M. Abo El-Hadeed *et al* 2025 *J. Phys.: Conf. Ser.* **3070** 012017

Effect of Sawtooth Current Waveform on Plasma Dynamics in Electrothermal PPT: A Simulation Approach

Marwa. M. Abo El-Hadeed[1*], M. A. Bourham[2], and M. A. Abd Al-Halim[1],

[1] Physics Department, Faculty of Science, Benha University, Benha, 13518 Egypt.
[2] Department of Nuclear Engineering, North Carolina State University, Raleigh, NC 27695-7909, USA.
* E-mail: marwa.aboelhadeed@fsc.bu.edu.eg

Abstract. The Increased attention toward pulsed plasma thrusters for satellite propulsion is due to their small size, simplicity, and low power consumption advantage. Electrothermal pulsed plasma thrusters are considered high-thrust engines. This research presents a theoretical study of the influence of the discharge current signal waveform on plasma parameters such as plasma temperature, exit pressure, and exit velocity. Furthermore, it examines the impact on thrusters' properties, such as the ablated mass from the wall of the capillary tube, besides the thrust, impulse, and specific impulse. The paper was conducted using a sawtooth signal and Teflon capillary to study the effect of fast abruption variation of the plasma parameters. Calculations are obtained using a 1-D time-dependent ETFLOW model, which describes the physical phenomenon of coaxial electrothermal discharge systems. Additionally, the paper includes an axial analysis of some properties, such as the exit pressure, velocity, and the plasma temperature inside the capillary.

1. Introduction

Pulsed plasma thrusters (PPTs) are prioritized as electric propulsion engines for small satellites in space missions such as station-keeping and altitude control [1, 2]. To reduce the consumed power, PPTs have become more appropriate for satellites than chemical or gas thrusters due to their simplicity, dependability, and compact size. In addition, they can achieve variable thrust and specific impulse using low-power energy [3].

Electrothermal Pulsed Plasma Thrusters (ETPPTs) are regarded as high-thrust electric propulsion engines since they produce greater thrust than electromagnetic thrusters [4].

The mechanism of generating thrust depends on the thermal expansion of plasma out of the capillary. The mechanism of generating thrust depends on the thermal expansion of plasma out of the capillary; the temperature from the is transferred to the inner wall of the capillary causing ablation and ionization raising the density of the plasma, hence, increasing the pressure causing pressure gradient inside the capillary expelled plasma out of propellant [5, 6]. Many types of propellants can be used with PPTs, such as solid, liquid, and gas propellants. Although liquid and gas propellants provide higher values of specific impulse, polytetrafluoroethylene (PTFE) is the most commonly utilized propellant because of its superior performance. It is appropriate for long and high-temperature operation because of its ability to resist flame and corrosion [7].

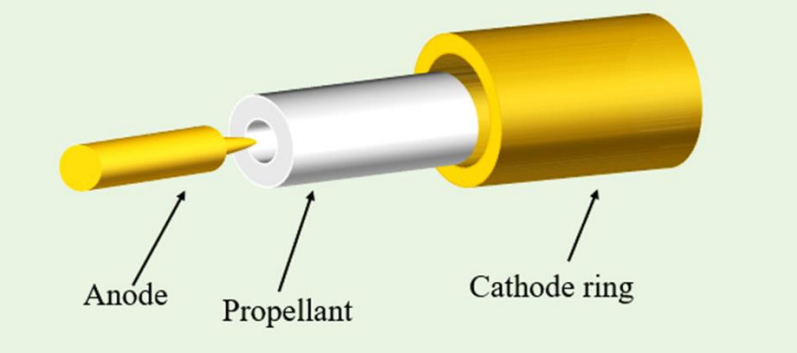

Figure 1. The capillary tube.

In the present research, a theoretical study was conducted to investigate the effect of the current signal on the behavior of plasma properties such as density, pressure, and velocity, besides the variation of the ablated mass. Consequently, its effect on thruster properties such as thrust, impulse, and specific impulse. In the second part, the study investigates physical properties such as pressure, temperature, and velocity as a function of the axial position along the capillary axis. The applied discharge current signal is the sawtooth waveform. Calculations are performed using the modified ETFLOW model for electrothermal capillary discharge, which includes equations of thruster performance such as thrust, impulse, and specific impulse, by using a Teflon capillary with a diameter of 4 mm and a length of 5 cm.

2. The Design of the Capillary Discharge

Figure 1 illustrates the electrothermal. The ET discharge capillary is connected to an inner tip anode, an outer annulus cathode, and the Teflon capillary between the two electrodes. The system is connected to the capacitor bank, switch, and power supply.

When the discharge begins, the radiation flux from the arc incidents on the inner wall of the Teflon capillary causes an ablation from the wall surface. The ablated molecules are dissociated by the heat and ionized, forming plasma. The ablation process is accompanied by an increase in the density, forming a pressure gradient that propels the plasma out of the capillary muzzle, generating the thrust [5, 6].

During the ablation phenomenon, the heat flux produced by the arc is absorbed by a highly dense vapor formed by the ablated molecules from the capillary so that only a portion of the heat flux is transmitted to the capillary wall, which is known as the vapor shield effect [8, 9]. Therefore, we used an equation for the transmission heat factor for polymers rather than using the ideal value of one. This value is confirmed in several published research [10, 11].

3. Assumptions of Model and Governing Equations:

The ETFLOW model used in this study is based on several essential assumptions that ease the calculations and give realistic results which are published in the previous publications [12-13]. These assumptions can be summarized as follows: the study is time-dependent, one direction, the effect of radial motion of plasma is negligible, and the viscous force from the boundary is negligible. Also, it is basically assumed that plasma is in local thermodynamic equilibrium so that Saha equation can be involved to describe plasma state. Moreover, heat transfer by

radiation mechanism is dominant, while heat transfer by conduction or convection is negligible. In addition, the ablation from the two electrodes is negligible and the plasma is expelled out of the capillary due to the high-pressure gradient force and there is no effect of the magnetic pressure. The model includes the vapor shield effect, so that, not all the radiation flux from the arc reaches the Teflon inner wall. Therefore, a modified equation for the transmission heat factor can be used.

The model depends on some general equations that describe the plasma motion such as conservation of the momentum, mass, and energy which describe the behavior of physical parameters of the electrothermal capillary discharge such as plasma density, temperature, velocity, pressure, ablated mass, internal energy and ionization of plasma species besides the thruster equations such as thrust, impulse and specific impulse.

3.1. Continuity equation:

The left-hand side of the equation demonstrates the rate of the plasma density change inside the capillary which is equal to the difference between the rate of ablation from the walls and the number density of particles that leave the capillary [12 - 15]:

$$\frac{\partial n}{\partial t} = \dot{n} - \frac{\partial (vn)}{\partial z} \tag{1}$$

Where v is the velocity of plasma (m/ s^2), n is the plasma number density (m^{-3}), and $\dot{n}$ is the rate of ablation ($m^{-3}.s^{-1}$) which is given by:

$$\dot{\mathrm{n}} = \frac{2\mathrm{q}}{\mathrm{R}\,\mathrm{H_{sub}}\mathrm{A_P}} \tag{2}$$

and $\mathrm{H_{sub}}$ is the specific heat of sublimation (J/kg), $\mathrm{A_P}$ is the mass of the atom which constitutes plasma (kg), and q is radiation heat flux (W/ m^2) [13, 14], which could be given by [12, 16]:

$$q = F_t \sigma_s \left(T^4 - {T_{vap}}^4\right) \tag{3}$$

Where σ_s is Stefan–Boltzmann constant, T is plasma temperature, $\mathrm{T_{vap}}$ is the vaporization temperature of the capillary, and $\mathrm{F_t}$ is the energy transmission factor (gray factor) which describes the amount of energy transferred to the inner wall of capillary tube.

3.2 Momentum equation:

It demonstrates that the rate of change in plasma velocity is produced by the pressure gradient, kinetic energy gradient, and the ablation process, which increases density.

$$\frac{\partial v}{\partial t} = -\frac{1}{\rho}\frac{\partial P}{\partial z} - \frac{1}{2}\frac{\partial v^2}{\partial z} - \frac{v\dot{n}}{n} \tag{4}$$

Where: ρ is the mass density of plasma (kg/m^3), R is the capillary radius (m), and P is the pressure (N/m^2)

3.3 Conservation energy equation:

The first term on the RHS is Joule heating, the second term refers to the loss in internal energy caused by thermal radiation, the third term is due to the work done by plasma, and the fourth term is the loss due to particles which enter or leave the capillary [12 -14].

$$\frac{\partial (nU)}{\partial t} = \eta j^2 - \frac{2q}{R} - P\frac{\partial v}{\partial z} - v\frac{\partial (nU)}{\partial z} \tag{5}$$

Where U is internal energy (J), j is current density (A/m^2), η is plasma resistivity ($\Omega.m$).

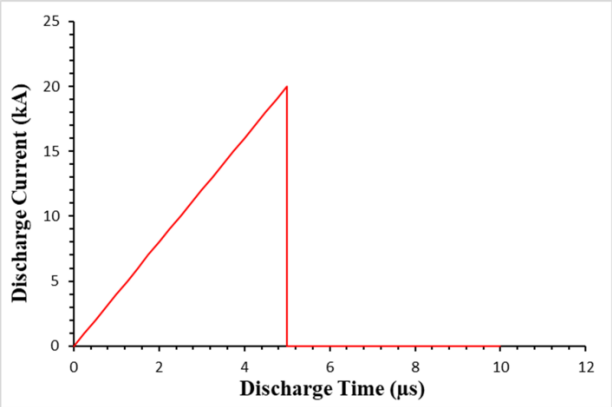

Figure 2. Discharge current signal.

3.4 Thrust and impulse equations:

Thrust (Γ) produced from plasma is given by the product of the flow rate of the ablated mass multiplied by the plasma exit velocity from the capillary muzzle [17, 18]. The integration of thrust over the discharge time is the impulse (I) and is given by [19, 20]:

$$\Gamma = \frac{dm}{dt}.v_{ex} \tag{6}$$

$$I_m = \int \Gamma dt = v_{ex}\int_0^{t_p}\frac{dm}{dt}\,dt \tag{7}$$

The specific impulse I_s is defined as the impulse per unit weight of propellant [18] and it is given by:

$$I_s = \frac{\int \Gamma dt}{g.\int_0^{t_p}\frac{dm}{dt}\,dt} \tag{8}$$

Where g is the acceleration due to gravity.

4. Results and Discussion

Figure 2 shows the discharge current signal in shape of sawtooth as used in the present calculations. The discharge current increases from until reaching the maximum value of 20 kA at 5 µs and then quickly drops to zero with a signal duration of 5 µs. The discharge is considered to take place in a Teflon capillary that is 5 cm in length and 4 mm in diameter.

4.1. Properties of Electrothermal Discharge and Plasma Propulsion:

Figure 3 depicts the behavior of the variation of the plasma temperature, plasma exit velocity, and radiation heat flux at the muzzle end with time. The figure shows that the temperature increases until it reaches the maximum value of 2.23 eV at time 5.1 µs. The radiation heat flux reaches the maximum value of 25.6 GW/m^2, while the plasma exit velocity reaches its maximum value of about 3.2 km/s at a time of 6.6 µs. A similar trend was conducted in [12, 10, 21, 22]

When the discharge occurs, the temperature inside the capillary rises accompanied by an increase in the radiation heat flux according to Eq.3. According to Eq.5, the increase of the temperature accompanied by the discharge current causes a rise in the internal energy inside the capillary, hence, the kinetic energy increases resulting in a rise of the exit the velocity. Although the discharge current drops rapidly at 5 µs, the temperature, heat flux, and exit velocity decrease gradually until nearly 20 µs, due to the longer time needed for cooling.

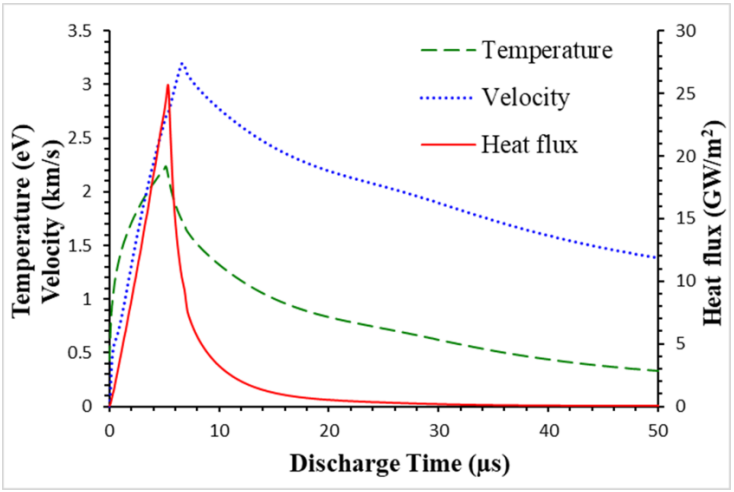

Figure 3. The behavior of temperature, heat flux, and velocity versus the discharge time.

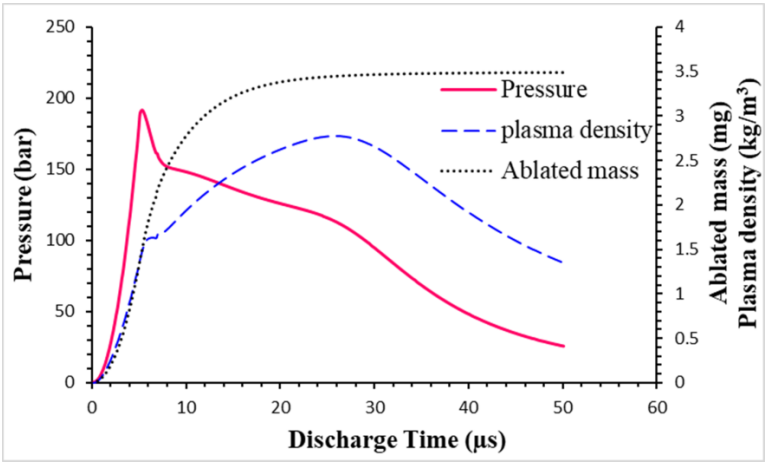

Figure 4. The variation of ablated mass, plasma density, and pressure with discharge time.

Figure 4 represents the change of the ablated mass per pulse, plasma density, and plasma density at the muzzle end with the discharge time. When the discharge occurs, the radiation heat flux from the arc increases inside the capillary, then according to Eq. 2, the ablated mass increases until it reaches the maximum value of about 3.4 mg after about 20 µs. Increasing the ablation is accompanied by a rise of the plasma density until it reaches the maximum value of 2.77 kg/m^3 at 25 µs. As a result, the pressure inside the capillary due to ablation and ionization processes reaches the maximum of 191.8 bar at 5.3 µs, resulting in a pressure gradient that propels plasma out of the muzzle end of the capillary tube. After the discharge ends at 5 µs, the temperature inside the capillary is still high enough to sustain the ablation process for a while. Consequently, the ionization and recombination processes persist for a while. Therefore, the ablated mass and plasma density reached the maximum value after a longer time in the arc. The behavior of parameters agrees with [6, 10, 12, 14, 23]

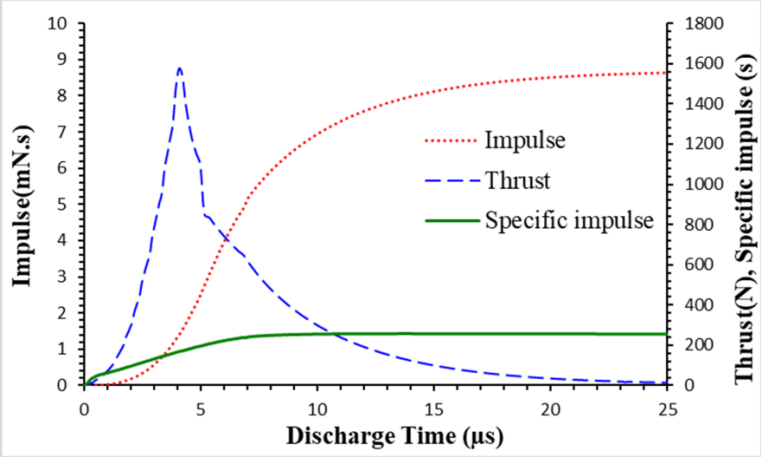

Figure 5. The behavior of thrust, impulse, and specific impulse with discharge time.

Figure 5 depicts the variation of thrust, impulse, and specific impulse as a function of the discharge time. The thrust raises and reaches the maximum value of 1575 N at 5.1 μs, which is synchronized with the time of both peaks of the discharge current and plasma temperature. Although the plasma density reached its peak at 25 μs, the thrust decayed and vanished at nearly 15 μs, because of the very low value of the mass variation term (dm/dt) according to Eq. 6. In addition, the impulse reaches the saturation value of 8.1 mN.s at a time of 15 μs and the specific impulse has a value of about 257 s. Similar trends were found by [6, 10, 21, 22]

4.2 Effect of the Transmission Heat Factor on Discharge Parameters:

In this part, one shows the effect of change of the transmission heat factor on the different calculated parameters from the model. The calculations of the previous part were conducted assuming the ideal value of the transmission heat factor (F_t=1). It was considered that plasma was ideal for black body radiation, and all heat radiated from the arc plasma was transferred to the inner wall of the capillary. Consequently, the calculated values are expected to be higher than the real values. Experimentally, not all radiation from the plasma is transferred to the inner wall of the capillary because the ablated mass from the walls can absorb part of the energy and only a fraction of heat flux reaches the inner wall. Therefore, the transmission heat factor was modified to agree with the experimental data.

In this part, we used a modified equation for transmission heat factor developed by Muller [25] which is suitable for use with organic polymers such as Teflon, and polyethylene [26]. The modified transmission heat factor equation is given by:

$$F_t = 1 - e^{-0.025(Pr)^{0.6}} \quad (9)$$

Where: P is the plasma pressure (bar), and r is the arc radius (mm). It was assumed that the plasma fills all parts of the capillary tube then r≈R.

Table 1 shows the effect of using the transmission heat factor from the Eq. 9 equation on physical quantities of plasma using the same Teflon capillary dimensions of 2 mm in radius and 5 cm in length. According to Eq. 3, using a modified transmission heat factor equation reduces the amount of heat flux, thus, reducing the amount of ablated mass according to Eq. 2. Therefore, this will cause a reduction in plasma density along with decreasing of the pressure value. According to Eq.6 and 7, decreasing the ablated mass causes a reduction in the amount of thrust and impulse. In contrast, a temperature rise is observed due to a decrease in the number of

Table 1. Comparison between values of the different parameters for the two cases of the heat transmission factor.

Quantity	f_t=1	f_t from Eq. 9
Heat flux (GW/m^2)	25.6	20.7
Mass (mg)	3.4	2.8
Plasma density (kg/m^3)	2.77	2.1
Pressure (bar)	191.8	155
Temperature (eV)	2.2	2.4
Velocity (km/s)	3.2	3.3
Thrust (N)	1575	1303
Impulse (mN.s)	8.1	7.5
Specific impulse (s)	257	273

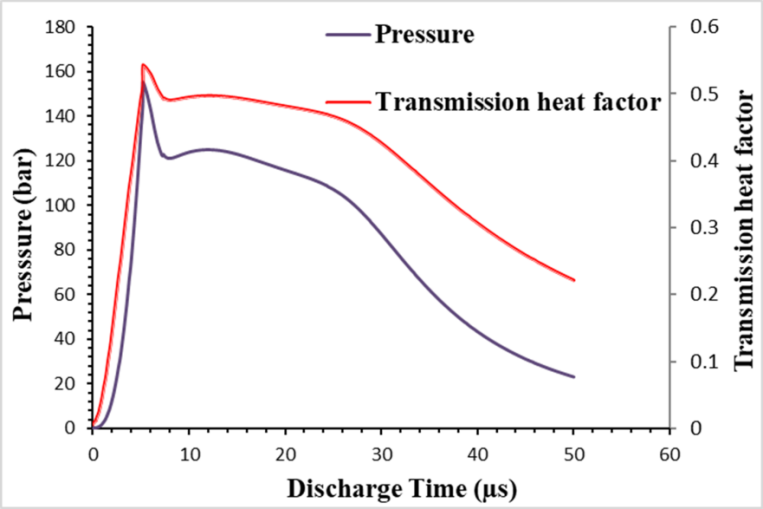

Figure 6. The variation of transmission heat factor with the discharge time.

collisions between particles. As a result, the plasma velocity increases, consequently, raising the amount of specific impulse.

Figure 6 represents the behavior of the transmission heat factor from Eq. 9 and pressure calculated in this case as a function of the discharge time. According to Eq. 9, the trend of the transmission factor depends on the pressure and has a similar behavior. The transmission factor increases with increasing pressure until it reaches the maximum value of about 0.54 at a time of 5.3 µs, which is synchronized with the time of the peak of pressure.

4.3 Axial Distribution of the Plasma Parameters Along the Capillary Axis:

In this part, plasma density, the pressure inside the capillary, and plasma velocity are studied as illustrated along the capillary axis for different discharge times. All parameters were studied for a capillary of 5 cm in length and 4 mm in diameter at discharge times of 2.5 µs, 5 µs, 10 µs, and

15 μs. In the present model, we divided the capillary into 11 nodes, where the first node is located at the anode tip and node 11 is located at the muzzle end of the capillary.

Figure 7 illustrates the change in plasma density along the capillary axis. It showed that plasma density near the tip always has the maximum value and starts to decrease as it gets closer to the muzzle end. The expansion of plasma out of the capillary reduces the plasma accumulation and plasma density at the muzzle. In addition, the density of plasma increases with time due to the effect of temperature and the input energy as discussed previously.

A similar behavior is observed for the variation of pressure along the capillary axis as illustrated in Fig. 8. The pressure has its maximum at the first node close to the anode tip and decreases reaching the minimum value at the muzzle end where the plasma leaves the capillary. This is the case for the discharge time up to 10 μs. Then, for 15 μs and beyond, the pressure in all regions decreases due to the lower heat flux after the end of the discharge. However, the pressure gradient still exists, where the pressure is higher at the inner region and gradually decreases towards the muzzle end.

Figure 9 shows the behavior of plasma velocity along the capillary axis. It is shown that velocity increased from the minimum value at the tip until it reached the maximum value at the muzzle end. According to the momentum equation Eq.4, increasing the pressure gradient and ablation process leads to a reduction in the plasma velocity, which is consistent with the behavior of the pressure distribution.

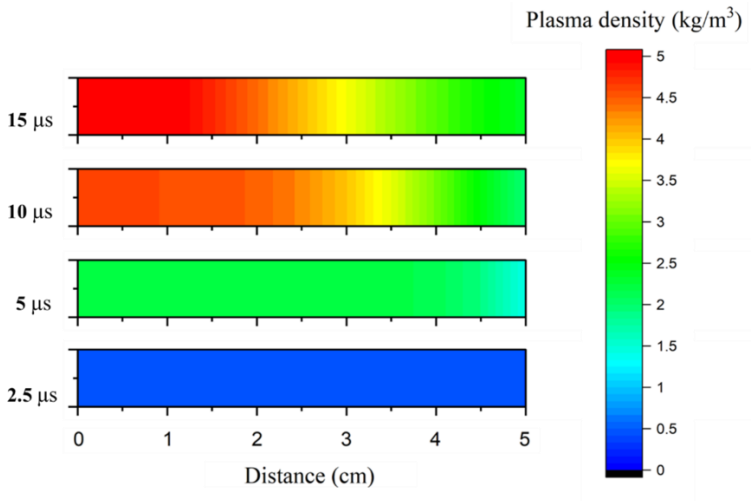

Figure 7. The behavior of plasma density along the capillary axis.

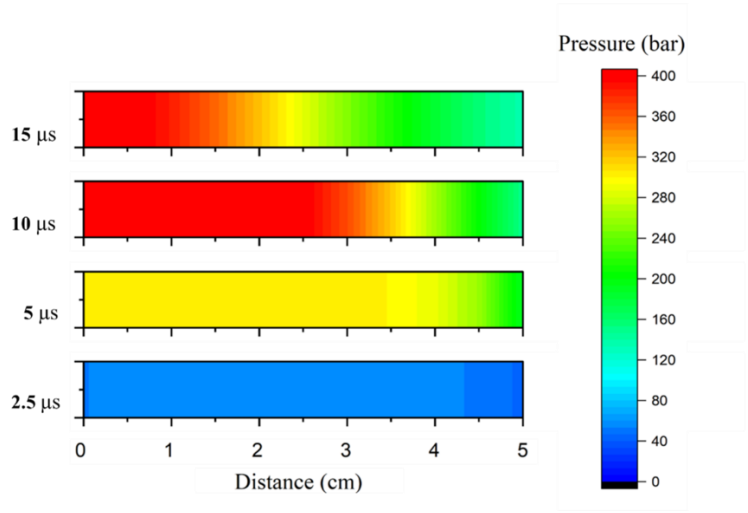

Figure 8. The variation of pressure along the capillary axis.

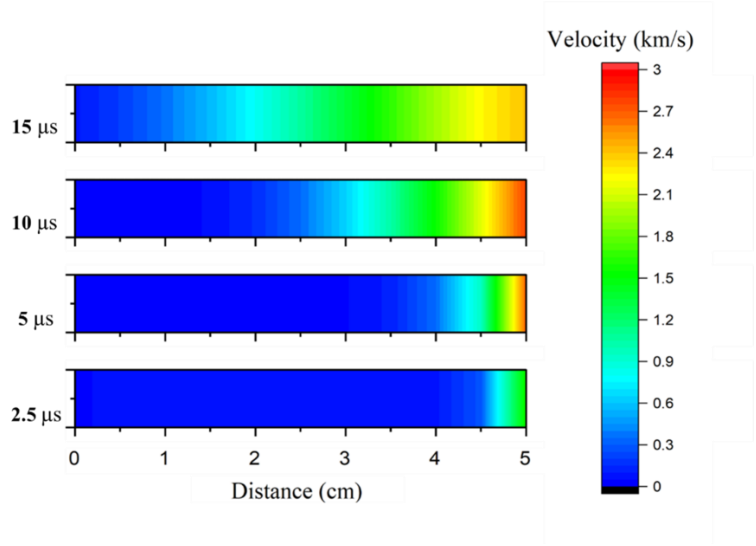

Figure 9. The behavior of plasma velocity along the capillary axis.

5. Conclusion

This work was carried out to simulate the effect of a sawtooth wave on the behavior of various physical parameters over the discharge time such as plasma density, plasma temperature, heat flux, and velocity, as well as thrust parameters such as Thrust, impulse, and specific impulse which describe the performance of electrothermal discharge using Teflon capillary. The calculations were carried out using the ETFLOW model, which is based on different essential equations such as mass conservation, momentum, and energy, in addition to the equations that describe the performance of thrusters such as the thrust, impulse, and specific impulse.

The study also includes an axial distribution of various parameters along the capillary length, such as plasma density, pressure, and plasma velocity. The final part of the study investigates the effect of using a modified transmission heat factor on the values of several physical parameters, such as ablated mass, pressure, density, temperature, thrust, impulse, and specific impulse. It was found that plasma does not treat as an ideal black body due to the shielding effect of ablated atoms, and transmission heat factor is a function of pressure and arc radius, so using the modified equation of transmission factor can give more realistic values, and will reduce the calculated ablated mass by 17.26% from 3.4 mg to 2.8 mg and pressure by 19 %, which consistently will reduce the thrust by the same ratio of ablated mass from 1575 N to 1303 N and impulse values from 8.1mN.s to 7.5 mN.s. In contrast, it increases the value of temperature from 2.2 eV to 2.4 eV and raises specific impulses.

References

[1] Burton, R. L., & Turchi, P. J. (1998). J. Propul. Power, 14(5), 716-735.
[2] Gessini, P., Habl, L. T., Barcelos Jr, M. N., Ferreira, J. L., Marques, R. I., & Coletti, M. (2013, October). 33rd Int. Electric Propulsion Conf. (Washington, DC) (pp. 2013-344).
[3] Zhiwen, W. U., Huang, T., Xiangyang, L. I. U., Ling, W. Y. L., Ningfei, W. A. N. G., & Lucheng, J. I. (2020), Plasma Sci. Technol., 22(9), 094014.
https://doi.org/10.1088/2058-6272/aba7ac
[4] Edamitsu, T., Asakura, H., Matsumoto, A., & Tahara, H. (2005, October). In 29th International Electric Propulsion Conference.
[5] Zhang, Z., Ling, W. Y. L., Tang, H., Cao, J., Liu, X., and Wang, N. (2019), Rev. Mod. Plasma Phys. Vol. 3, pp. 1-41.
https://doi.org/10.1007/s41614-019-0027-z
[6] Mikellides, P., and Turchi, P. (1996), 32nd Joint Propulsion Conference and Exhibit, Florida, USA, p. 2733.
https://doi.org/10.2514/6.1996-2733
[7] Ou, Y., Wu, J., Du, X., Zhang, H., & He, Z. (2019). Vacuum, 165, 163-171.
https://doi.org/10.1016/j. Vacuum.2019.04.027
[8] Gilligan, J. G., and Mohanti, R. B. (1990), IEEE Trans. Plasma Sci., Vol. 18, No. 2, pp. 190-197.
https://doi.org/10.1109/27.131019
[9] Gilligan, J., Hahn, D., and Mohanti, R. (1989), J. Nucl. Mater. Vol. 162, pp. 957-963.
https://doi.org/10.1016/0022-3115(89)90393-0
[10] Abo El-Hadeed, M. M., Bourham, M. A., & Abd Al-Halim, M. A. (2024). IEEE Trans. Plasma Sci.https://doi.org/10.1109/TPS.2024.3502626
[11] Abid, F., Niayesh, K., & Støa-Aanensen, N. S. (2018). IEEE Trans. Plasma Sci., 47(1), 754-761.
https://doi.org/10.1109/TPS.2018.2880841
[12] Abdel-Kader, M. E., Abd Al-Halim, M. A., and Bourham, M. A. IEEE Trans. Plasma Sci., Vol. 46, No. 6, 2018, pp. 2099-2107.
https://doi.org/10.1109/TPS.2018.2829108
[13] Hurley, J. D., Bourham, M. A., and Gilligan, J. G. (1995), IEEE Trans. Magn. Vol. 31. No. 1, pp. 616-621.
https://doi.org/10.1109/20.364624
[14] Winfrey, A. L., Abd Al-Halim, M. A., Gilligan, J. G., Saveliev, A. V., and Bourham, M. A. (2012), IEEE Trans. Plasma Sci., Vol. 40, No. 3, pp. 843-852.
https://doi.org/10.1109/TPS.2011.2179985
[15] Mohanti, R. B., and Gilligan, J. G. (1993), IEEE Trans. Magn. Vol. 29, No. 1, pp. 585-590.
https://doi.org/10.1109/20.195641
[16] Abd Al-Halim, M. A., and Bourham, M. A. (2018), Plasma Phys. Rep. Vol. 44, pp. 870-877.
https://doi.org/10.1134/S1063780X18090015
[17] Sforza, P. M. (2016), 2nd ed. Butterworth-Heinemann, Netherlands, Chap. 13.

[18] Schoenherr, T., and Komurasaki, K. Sep. 2011, 32nd International Electric Propulsion Conference, IEPC-2011-340, Wiesbaden, Germany.
[19] Greenwood, S. W. (1975), J. Spacecr. Rockets, Vol. 12, No. 1, pp. 62-62.
https://doi.org/10.2514/3.27809
[20] Marquart, E., and Coulter, S. (1998), 36th AIAA Aerospace Sciences Meeting and Exhibit, Nevada, USA, p. 203.
https://doi.org/10.2514/6.1998-203
[21] Edamitsu, T., and Tahara, H. (2005), 29th International Electric Propulsion Conference, IEPC-2005-105, Princeton University, USA.
[22] Cambier, J., Young, M., Pekker, L., and Pancotti, A. (2007), International Electric Propulsion Conference, IEPC-2007-238, Florence, Italy, pp. 2007-238.
[23] Ishii, Y., Takagi, H., and Tahara, H. (2009), 31st International Electric Propulsion Conference., IEPC-2009-253, University of Michigan, USA.
[24] Tanaka, M., Kisaki, S., Ikeda, T., and Tahara, H. (2012), IEEE Vehicle Power and Propulsion Conference, IEEE, pp. 517-522.
https://doi.org/10.1109/VPPC.2012.6422747
[25] Muller, L. (1993). J. Phys. D: Appl. Phys. Vol. 26, No. 8, pp. 1253.
https://doi.org/10.1088/0022-3727/26/8/015
[26] Niemeyer, L. (1978). IEEE Trans. Power App. Syst., Vol. 3, pp. 950-958.
https://doi.org/10.1109/TPAS.1978.354568